

Dynamical mass generation in unquenched QED using the Dyson–Schwinger equations

Ayşe Kızılersü,^{1,*} Michael R. Pennington,^{2,†} Tom Sizer,^{1,‡} Anthony G. Williams,^{1,3,§} and Richard Williams^{4,¶}

¹*Special Research Centre for the Subatomic Structure of Matter,
School of Chemistry and Physics, Adelaide University, 5005, Australia*

²*Thomas Jefferson National Accelerator Facility, Newport News, Virginia 23606, USA*

³*ARC Centre of Excellence for Particle Physics at the Tera-scale,
School of Chemistry and Physics, Adelaide University, 5005, Australia*

⁴*Institut für Theoretische Physik, Justus-Liebig-Universität Gießen, 35392 Gießen, Germany*

(Dated: September 23, 2014)

We present a comprehensive numerical study of dynamical mass generation for unquenched QED in four dimensions, in the absence of four-fermion interactions, using the Dyson–Schwinger approach. We begin with an overview of previous investigations of criticality in the quenched approximation. To this we add an analysis using a new fermion-antifermion-boson interaction ansatz, the Kızılersü–Pennington (KP) vertex, developed for an unquenched treatment. After surveying criticality in previous unquenched studies, we investigate the performance of the KP vertex in dynamical mass generation using a renormalized fully unquenched system of equations. This we compare with the results for two hybrid vertices incorporating the Curtis–Pennington vertex in the fermion equation. We conclude that the KP vertex is as yet incomplete, and its relative gauge-variance is due to its lack of massive transverse components in its design.

PACS numbers: 11.15.Ex, 12.20.-m, 12.38.Cy

I. INTRODUCTION

Quantum Electrodynamics has served as a prototype field theory for studying both perturbative and non-perturbative phenomena for many years. Though the coupling constant in nature is small, and hence perturbative expansions meaningful, one can imagine a theory of strongly-coupled QED where such an approach is inappropriate. The attraction of looking at such a scenario lies with its relatively simple Abelian gauge structure and fermion-antifermion-photon interaction: QCD, by way of contrast, although naturally exhibiting a strong-coupling regime, is non-Abelian and requires knowledge of the quark-gluon [1–3] and three-gluon vertices [4–6].

Essentially, there are two mainstream approaches to non perturbative studies of QED: those on the lattice and those using a continuum approach such as the Dyson–Schwinger Equations. Finite volume calculations on the lattice tend to concentrate on the three-dimensional variant, where the phase structure of the theory is of interest not only because of its analogies to QCD, but also for its potential application to the study of cuprate superconductors. Functional methods have found that finite volume effects are large [7, 8], which is significant for more realistic models featuring anisotropy [9–11]. Though lattice studies have looked at the four dimensional case, there has been little progress over the last few years due to complications associated with the four-fermion opera-

tor. This causes difficulties when comparing lattice studies with pure QED as calculated using the continuum approach.

A key component in developing our understanding of non-perturbative physics has been the study of the mechanism of dynamical mass generation. The DSE approach to this is to calculate the fermion and photon propagators numerically. This requires knowledge of the fermion-photon vertex, which can either be provided by Ansatz or calculated from its DSE. In the absence of a bare mass, it is universally found that the fermion mass function is non-zero only above some critical value of the coupling. The majority of these studies have been limited to the quenched theories [12–39] where the photon propagator is tree-level and the coupling does not run: only few works have been devoted to the unquenched (complete) theory [27–29, 40–51]. This has historically involved two limitations - the computational challenge recently ameliorated by the emergence of faster computers, and the incomplete knowledge of the explicit form of the 3-point fermion-photon Green’s function (the vertex). Today, progress has been made towards directly solving the vertex DSEs, with most of the attention focused upon QCD [2, 5, 6, 52–54]. However, complementary to this is the explicit construction of vertex models constrained by consideration of functional identities [3, 4, 55].

In this paper we present a comprehensive study of dynamical mass generation in strong coupling four dimensional QED using the DSEs. The numerical analysis has been performed independently by two groups, MRP and RW [29], and AK, TS and AGW [51, 56]. We report jointly upon a recent Ansatz [57], dubbed the Kızılersü–Pennington vertex (KP), and explore its properties as a function of coupling strength, gauge parameter, and fermion number. The paper is organized as

* akiziler@physics.adelaide.edu.au

† michaelp@jlab.org

‡ tsizer@physics.adelaide.edu.au

§ anthony.williams@adelaide.edu.au

¶ richard.williams@theo.physik.uni-giessen.de

follows. In section II the DSE formalism is introduced, followed by a discussion of multiplicative renormalizability and its importance, section III. Two fermion-photon vertices constrained by this are presented, that of Curtis–Pennington (CP) vertex for quenched QED [58] and the KP vertex for unquenched QCD. In section IV we give a numerical survey of the critical fermion number in quenched massless QED₄ and compare to the KP vertex. Strictly massless solutions with the unquenched KP vertex are presented in section V. Fermion flavour criticality and dynamical mass generation for a variety of gauges is discussed in section VI, where hybrid vertex models that incorporate the CP vertex in the fermion equation are also studied. We conclude in section VII.

II. DYSON–SCHWINGER EQUATIONS

In a Quantum Field Theory, all fundamental quantities may be related to the underlying Green’s functions that describe the theory. In Euclidean space, where with almost no exception non-perturbative calculations are performed, the equations of motion describing these correlation functions are the Dyson–Schwinger Equations (DSEs). The lowest order DSEs relevant to QED are shown in Fig. 1. These are the first of an infinite tower of coupled non-linear integral equations, relating Green’s functions of different orders. Each of these with N_F fermion legs and N_A photon legs satisfies its own equation. These couple each one-particle irreducible Green’s function to others as illustrated in Fig. 1 and take the form of non-linear integral equations. The DSEs for two point functions (the fermion and photon propagators) are shown in Fig. 1 and given explicitly in Eqs. (1, 2) to come. To solve the infinite tower is impossible, consequently, some form of truncation must be introduced. Minimally, to evaluate the two point functions, we need to introduce a suitable Ansatz for the fermion-photon vertex that appears in both of the equations in Fig. 1. To be realistic, such an Ansatz must attempt to encode the effect of all the higher point Green’s functions, at least as far as their implication for the fermion and photon propagators is concerned. The treatment discussed in section III is an example of this.

A. Fermion and Photon Propagators

The renormalized DSEs for the fermion and photon propagators are

$$\begin{aligned} S^{-1}(p) &= Z_2 S^{(0)-1}(p) \\ &\quad - \frac{Z_2^2}{Z_1} ie^2 \int_M^\Lambda \widetilde{dk} \Gamma^\mu(p, k; q) S(k) \gamma^\nu \Delta_{\mu\nu}(q), \\ \Delta_{\mu\nu}^{-1}(q) &= Z_3 \Delta_{\mu\nu}^{(0)-1}(q) \end{aligned} \quad (1)$$

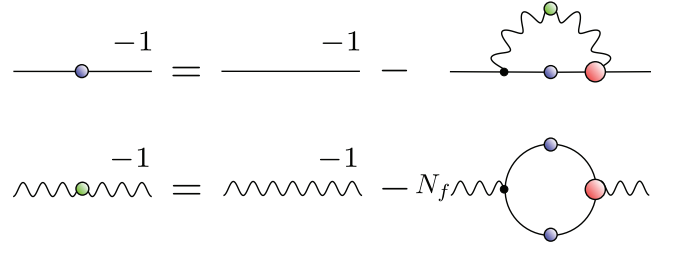


FIG. 1. The Dyson–Schwinger Equations in QED for the fermion and photon propagators (straight and wavy lines respectively). Full circles denote fully dressed quantities.

$$+ \frac{Z_2^2}{Z_1} ie^2 N_F \text{Tr} \int_M^\Lambda \widetilde{dk} \Gamma_\mu(p, k; q) S(k) \gamma_\nu S(p). \quad (2)$$

Here $\widetilde{dk} = d^4k/(2\pi)^4$, $q = k - p$, $S^{(0)}$ and $\Delta_{\mu\nu}^{(0)}$ are the tree-level fermion and photon propagators respectively, and the Z_i factors relate the unrenormalized quantities arising from the Lagrangian to the corresponding renormalized quantities appearing in these equations. Renormalization allows us to trade the momentum cut-off Λ for some physical renormalization point μ , so $Z_i = Z_i(\mu^2, \Lambda^2)$.

Explicitly, these relations are

$$\Gamma_\mu(k, p; \mu) = Z_1 \Gamma_\mu^0(k, p; \Lambda) \quad (3)$$

for the fermion-photon vertex,

$$S(p; \mu) = Z_2^{-1} S^0(p; \Lambda), \quad (4)$$

$$D_{\mu\nu}(q; \mu) = Z_3^{-1} D_{\mu\nu}^0(q; \Lambda), \quad (5)$$

for the fermion and photon propagators, and

$$\alpha(\mu) = (Z_2/Z_1)^2 Z_3 \alpha_0, \quad (6)$$

for the renormalized coupling strength, where $\alpha_0 = e_0^2/4\pi$ and $\alpha = e^2/4\pi$, and unrenormalized quantities in the preceding paragraph are indicated by a 0 superscript or subscript.

As is well-known, the Dirac structure of the fermion propagator can be decomposed as

$$S(p) = \frac{F(p^2)}{\not{p} - M(p^2)} = \frac{1}{A(p^2) \not{p} - B(p^2)}, \quad (7)$$

which implies

$$F(p^2) = \frac{1}{A(p^2)}, \quad M(p^2) = \frac{B(p^2)}{A(p^2)}. \quad (8)$$

While the fermion propagator comprises two gauge-dependent scalar functions, $F(p^2)$, the fermion wave-function renormalization function, and $M(p^2)$, the mass function, the full photon propagator is characterised by

one gauge-independent function, $G(p^2)$, the photon wave function renormalization,

$$\Delta_{\mu\nu}(q) = \frac{-1}{q^2} \left[G(q^2) \left(g_{\mu\nu} - \frac{q_\mu q_\nu}{q^2} \right) + \xi \frac{q_\mu q_\nu}{q^2} \right], \quad (9)$$

where ξ is the covariant gauge parameter. The gauge parameter is also renormalized via $\xi_0 = Z_\xi \xi$, from which the invariance of $\alpha\xi$ implies $Z_\xi = Z_3$.

The respective tree-level propagators are obtained by setting $A = G = 1$ and $B = m_0$ in the above, with m_0 the bare fermion mass appearing in the Lagrangian.

In this Abelian theory, the fermion-photon vertex must satisfy the Ward-Green-Takahashi identity (WGTI) [59–61]:

$$Z_1 q_\mu \Gamma^\mu(p, k) = Z_1 q_\mu \Gamma_L^\mu(p, k) = Z_2 S^{-1}(k) - Z_2 S^{-1}(p). \quad (10)$$

This plays a role in constraining the explicitly gauge-dependent part of the fermion DSE. The corresponding equation for the unrenormalized quantities results in the identification

$$Z_1 = Z_2, \quad (11)$$

so Eq. (6) simplifies to

$$\alpha(\mu^2) = Z_3 \alpha_0. \quad (12)$$

The renormalization point invariant running coupling is then given by

$$\alpha(p^2) = \alpha(\mu^2) G(p^2, \mu^2), \quad (13)$$

with G the photon dressing function. The mass function $M(p^2)$ is also a renormalization point invariant. An important consequence of the gauge symmetry is that the photon dressing function G is independent of the gauge parameter ξ , which itself receives no higher-order corrections.

B. Fermion-Photon Vertex

The fermion-photon vertex consists of twelve spin amplitudes built from I, γ^μ and two independent four-momenta, k^μ and p^μ . These can be combined into four longitudinal components, L_i , whose coefficient functions λ_i are wholly determined by the WGTI as Ball and Chiu stated [62], and eight transverse components T_i satisfying

$$q_\mu T_i^\mu(p, k) = 0; \quad T_i^\mu(k, k) = 0, \quad (14)$$

(that is, they are orthogonal to the photon momentum and free of kinematic singularities) such that

$$\Gamma^\mu(p, k) = \sum_{i=1}^4 \lambda_i L_i^\mu(p, k) + \sum_{i=1}^8 \tau_i T_i^\mu(p, k), \quad (15)$$

where $\lambda_i = \lambda_i(p^2, k^2, q^2)$ and $\tau_i = \tau_i(p^2, k^2, q^2)$. We employ the same basis for L_i as in [57, 63]:

$$\begin{aligned} L_1(p, k) &= \gamma^\mu, \\ L_2(p, k) &= (\not{k} + \not{p})(k + p)^\mu, \\ L_3(p, k) &= (k + p)^\mu, \\ L_4(p, k) &= (k^\nu + p^\nu) \sigma^{\mu\nu}, \end{aligned} \quad (16)$$

with $\sigma_{\mu\nu} = \frac{1}{2} [\gamma_\mu, \gamma_\nu]$. The longitudinal components are fixed uniquely by the WGTI to be (superscript ‘M’ denotes Minkowski space)

$$\begin{aligned} \lambda_1^M(p^2, k^2) &= \frac{1}{2} [A_k + A_p], \\ \lambda_2^M(p^2, k^2) &= \frac{1}{2} \frac{1}{(k^2 - p^2)} [A_k - A_p], \\ \lambda_3^M(p^2, k^2) &= -\frac{1}{k^2 - p^2} [B_k - B_p], \\ \lambda_4^M(p^2, k^2) &= 0, \end{aligned} \quad (17)$$

where $A_k = A(k^2)$ is a convenient shorthand. For the transverse basis, we content ourselves with considering only those components that are non-vanishing perturbatively in the massless limit:

$$\begin{aligned} T_2^\mu(p, k) &= [p^\mu (k \cdot q) - k^\mu (p \cdot q)] (\not{k} + \not{p}), \\ T_3^\mu(p, k) &= q^2 \gamma^\mu - q^\mu \not{q}, \\ T_6^\mu(p, k) &= \gamma^\mu (p^2 - k^2) + (p + k)^\mu \not{q}, \\ T_8^\mu(p, k) &= -\gamma^\mu k^\nu p^\lambda \sigma_{\nu\lambda} + k^\mu \not{p} - p^\mu \not{k}. \end{aligned} \quad (18)$$

The remainder of this paper is devoted to considering solutions of the DSE resulting from different choices of vertex arising from various forms for these transverse components $\tau_i(k, p)$. The chief ingredients will be the matching to perturbation theory in the appropriate limit and the preservation of multiplicative renormalizability by the truncation scheme.

III. MULTIPLICATIVE RENORMALIZABILITY AND CHOICE OF VERTEX

Early on in the course of investigating possible vertex truncations in the Dyson–Schwinger equations, it was noted that multiplicative renormalizability was not guaranteed to be preserved [58, 64, 65]. Indeed, whilst not surprising in the case of a bare vertex this problem remains even on adoption of the Ball–Chiu form for the fermion-photon vertex. It became apparent that to satisfy this necessary property of the equations, one must include a transverse part in the vertex. However, the WGTI does not furnish us with any information here so we must find other means to constrain these transverse components.

1. Curtis–Pennington Vertex

One approach to obtain non-perturbative constraints on the transverse part of the vertex is to use perturbation theory, and demand that the leading and sub-leading logarithms contained within our wave-function renormalization and mass functions re-sum correctly. This was the guiding principle taken by Curtis and Pennington [58] that led to the following form for the transverse part of the vertex in quenched QED: all $\tau_i = 0$, except

$$(\tau_6)^M = -\frac{\lambda_2^M(p^2, k^2)(k^2 + p^2)(k^2 - p^2)}{(k^2 - p^2)^2 + [M^2(k^2) + M^2(p^2)]^2}. \quad (19)$$

Numerical studies employing the Curtis–Pennington (CP) vertex showed that not only were the equations manifestly multiplicatively renormalizable for large values of the coupling, but also that they exhibited a much milder violation of gauge invariance [23] in critical studies. The success of this vertex and the lack of any further developments over the years means that it has been employed in many studies, from QED in three dimensions [66, 67] to studies of QCD [68, 69].

2. Kızılersü–Pennington Vertex

The Kızılersü–Pennington (KP) vertex [57] is an unquenched vertex in the sense that it has the right structure to satisfy both fermion and photon DSEs. Moreover it respects gauge invariance, multiplicative renormalizability, agrees with perturbation theory in the weak coupling limit and is free of kinematic singularities. The appearance of logarithms of the fermion finite renormalization function $A(p^2)$ here are a result of the requirement that, for a perturbative expansion in the coupling, the coefficients of the leading logarithms exhibit the correct dependence on one another. The KP vertex has the following construction for the four unknown transverse form factors:

$$\begin{aligned} \tau_2^E &= -\frac{4}{3} \frac{1}{(k^4 - p^4)} (A_k - A_p) \\ &\quad - \frac{1}{3} \frac{1}{(k^2 + p^2)^2} (A_k + A_p) \ln \left[\left(\frac{A_k A_p}{A_q^2} \right) \right], \\ \tau_3^E &= -\frac{5}{12} \frac{1}{(k^2 - p^2)} (A_k - A_p) \\ &\quad - \frac{1}{6} \frac{1}{(k^2 + p^2)} (A_k + A_p) \ln \left[\left(\frac{A_k A_p}{A_q^2} \right) \right], \\ \tau_6^E &= \frac{1}{4} \frac{1}{(k^2 + p^2)} (A_k - A_p), \\ \tau_8^E &= 0, \end{aligned} \quad (20)$$

where ‘E’ denotes Euclidean space, and the momentum arguments of the $\tau_i^E(p^2, k^2, q^2)$ have been suppressed. A_k is a convenient shorthand for $A(k^2)$. Later we adopt a similar shorthand for $\alpha(\mu^2)$ of α_μ .

IV. QUENCHED QED₄ AND DYNAMICAL MASS GENERATION

If we ignore the contribution of fermion loops to the photon propagator, in effect quenching the theory, the coupling no longer depends on the photon momentum. A consequence of this truncation is that we do not need to consider the renormalization of the theory, since the only scale that enters the problem is the numerical cut-off Λ . It then makes sense to work in terms of dimensionless quantities $\hat{p}^2 = p^2/\Lambda^2$ and $M(\hat{p})/\Lambda$. Despite this displeasing scale dependence, the same constraints of multiplicative renormalizability may still be formally applied.

In this section, we consider three different choices of fermion-photon vertex; the bare vertex, the Curtis–Pennington vertex and the Kızılersü–Pennington vertex. The last two vertices include the Ball–Chiu construction as the longitudinal vertex. To study the impact of the truncation scheme (i.e vertex Ansatz and cutoff regulator) on the breaking of gauge invariance, we perform our calculations in three representative gauges, $\xi = 0, 1, 3$, and examine the behaviour of the critical coupling. Only Eqs. (A4, A6) of the DSEs need to be solved, since $G = 1, N_F = 0$ in the quenched approximation.

A. Previous Studies

Dynamical mass generation in strongly coupled QED in 3- and 4- dimensions has been historically of great interest. However the majority of the previous studies in the literature have been limited to the quenched approximation of the theory. The advantage of this approximation is that one can study the dynamical fermion mass generation analytically as well as numerically with some vertex approximations. Undeniably the results and guidance provided by these studies have been very valuable in developing our understanding of the phenomena of dynamical mass generation and for advancing the investigation of the robustness, performance and reliability of the numerical treatment [27–29, 70].

We now discuss some of the outcomes of these studies [12–38] in 4-dimensional quenched QED. The quenched DSE investigation of dynamical mass generation suggests that QED₄ undergoes a phase transition at a critical coupling α_c , when the interaction is strong enough. In the absence of a bare mass in the Lagrangian, the fermions in the theory are massless for all couplings less than this critical value ($\alpha < \alpha_c$), while they acquire mass for couplings greater than the critical one ($\alpha > \alpha_c$). The value of this critical coupling strongly depends on the truncation of the system [13, 14, 17–29, 31–35, 46] and which fermion-photon vertex is used. Furthermore it should be gauge independent [22, 28–31, 71] since it is (at least, in principle) a physical quantity.

In the very close vicinity of the critical point the dynamically generated mass admits a power-law behaviour [72] in Euclidean space, $M(p^2) = (p^2)^{-s}$, since

TABLE I. Critical couplings from previous studies for three different vertex Ansätze for $\xi = 0, 1, 3$ in quenched QED. The * vertex superscript indicates those solutions derived by applying the WGTI. ('NA' indicates 'not available'.)

ξ	0	1	3	Vertex
Ref. [13]	$\pi/3$	NA	NA	Bare
Ref. [23]	$1.003^* \pi/3$	NA	NA	Bare
Ref. [28]	1.047	1.690	2.040	Bare
Ref. [23]	0.9344	0.9240	0.9218	CP
Ref. [22]	0.933667	0.923439	0.921272	CP
Ref. [28]	0.933667	0.890712	0.832927	CP*
Ref. [31]	0.934	NA	NA	BBCR Ansatz

the SD system in quenched QED₄ is scale invariant. The exponent, s , which determines the asymptotic behaviour of the mass function is related to the anomalous dimension of the $\bar{\Psi}\Psi$ operator. Although this operator is not relevant in the perturbative region of QED₄ where it violates the renormalizability of the theory, it becomes large and renormalizable in the nonperturbative region; hence it becomes a relevant operator in non-perturbative DSE studies [37, 73–75]. This implies a four-fermion interaction with associated coupling parameter needs to be added to the theory. Such operators are automatically included in lattice calculations which makes it difficult to compare lattice studies directly with the SD calculations that do not include such an interaction term. Nevertheless lattice studies qualitatively support the DSE findings of quenched QED₄ by observing that the theory goes through a phase transition breaking chiral symmetry with associated dynamically generated mass [19, 76–82]. All of these studies agree that the dynamically generated mass obeys a mean field scaling law.

Table I shows critical couplings collected from various quenched QED₄ Dyson–Schwinger studies employing various vertices and using cutoff regularization. A few comments are in order. Miransky [13] demonstrated analytically that dynamical mass generation occurs in Rainbow QED (quenched QED with a bare vertex) in Landau gauge with a critical coupling of $\pi/3$. This was confirmed numerically by the other Rainbow studies cited. However, the use of the bare vertex makes the critical coupling highly gauge dependent, not least since it does not respect the WGTI. The development of the CP vertex led to the numerical study of [23] and the analytic study of [22], in substantial agreement, and exhibiting a reduced gauge dependence of the critical coupling. However, it emerged that using a cutoff regulator potentially violates the translation invariance of the theory, and leads to an ambiguity in the fermion DSE equation (except in Landau gauge), depending on whether or not the WGTI was applied in its derivation [22, 23], which was resolved using dimensional regularization [70] in favour of the former scenario. This accounts for the differing results for the CP vertex for $\xi \neq 0$ in Table I. Curiously, solutions for the CP vertex with the WGTI identity (correctly) ap-

plied exhibit greater gauge dependence than those where it is not applied.

In summary, quenched QED using the bare and CP vertex is now well understood. However, inspection of Table I reveals that the desired gauge independence of the critical coupling has only been partially realized, although the CP vertex represents a considerable improvement over the bare vertex [23].

B. Numerical Results for the Quenched KP Vertex

Here, we study the critical behaviour of quenched QED₄ using the Kızılersü-Pennington vertex [29, 57] in various gauges, comparing it with the bare and CP vertices. Only Eqs. (A4, A6) of the DSEs need to be solved, since $G = 1, N_F = 0$ in the quenched approximation. We show our results in Fig. 2 by plotting the dynamically generated Euclidean mass versus the coupling for $\xi = 0, 1, 3$. We expect the Euclidean mass near criticality to be only approximately gauge invariant since it is different than the physical mass which should be exactly gauge-independent : however the location of the critical coupling should be gauge invariant. Both solutions with and without application of the WGTI were run: Fig. 2 shows those without the WGTI. In these studies the momentum cut-off is $\Lambda^2 = 10^{10}$. For comparison purposes, we repeat these calculations using the bare and CP vertices.

Since the mass-function exhibits an infinite order phase transition, the measure of dynamical mass generation obeys the Miransky scaling law [18]. When the coupling is greater but very close to its critical value, we have

$$\frac{\Lambda}{m_E} = \exp \left(\frac{A}{\sqrt{\frac{\alpha}{\alpha_c} - 1}} - B \right), \quad (21)$$

where A, B and α_c can be determined through a least-squares fit. We summarize these critical couplings in Table II which show the results for solutions with the WGTI applied.

Figure 3 shows the dynamically generated mass versus coupling for the CP vertex for $\xi = 0, 0.25, 0.5, 1$, with fit parameters m, c, α_c and b in the formula

$$\frac{m_E}{\Lambda} = m \exp \left[-\frac{c}{(\alpha/\alpha_c - 1)^b} \right]. \quad (22)$$

TABLE II. Critical couplings for three different vertex Ansätze for $\xi = 0, 1, 3$ in quenched QED, with the WGTI applied. The Miransky scaling law, Eq. (21), is used to extract α_c . These results were generated by the Durham group [29].

ξ	0	1	3	Vertex
α_c	1.0472	1.690	2.040	Bare vertex
α_c	0.9339	0.8909	0.8329	Curtis–Pennington
α_c	0.9351	0.7222	$\simeq 0.5$	Kızılersü–Pennington

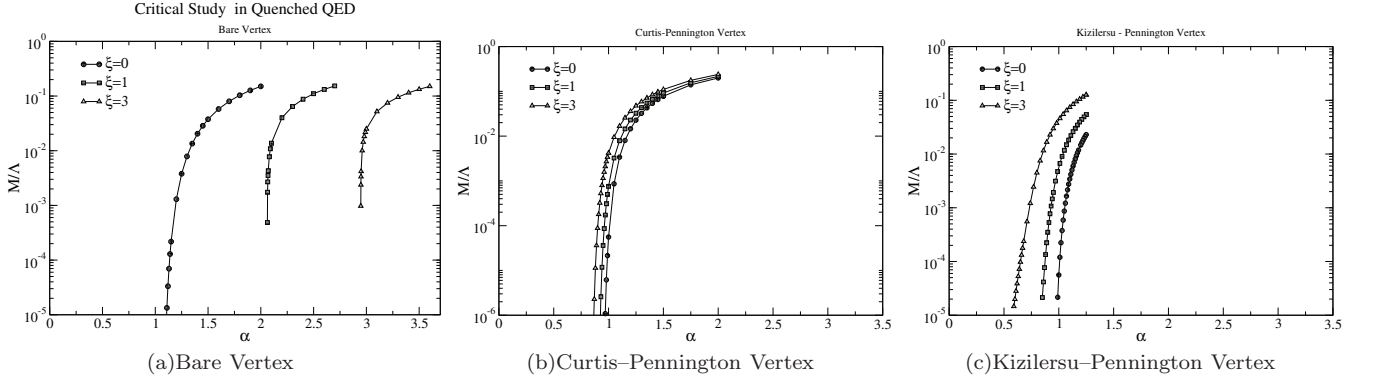


FIG. 2. Dynamically generated Euclidean mass versus coupling for $\xi = 0, 1, 3$ using the bare, Curtis-Pennington and Kızılersü-Pennington vertices respectively, without the WGTI.

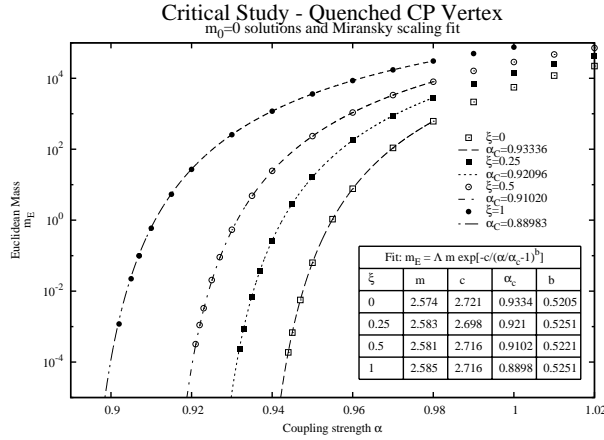


FIG. 3. Dynamical mass versus coupling for $m_0 = 0$ solutions in quenched QED₄ for gauges $\xi = 0, 0.25, 0.5, 1$ using the CP vertex with WGTI.

It is apparent that both the CP and KP vertices outperform the bare vertex, though the CP vertex has the smallest degree of gauge variance of the three models considered. Note that as the gauge parameter increases, the value of the critical coupling decreases for the CP and KP vertices, and increases for the bare vertex.

V. MASSLESS UNQUENCHED QED₄

Introducing fermion loops into the Dyson-Schwinger equation for the photon propagator leads to a running of the coupling. Renormalization then becomes mandatory, allowing us to trade the cut-off Λ for some physical renormalization point, μ .

Before investigating the effects of dynamical mass generation by examining critical behaviour, we investigate the strictly massless theory. Our primary purpose is to quantify the gauge-dependence of the photon dressing function $G(p^2)$, which should ideally be independent of

ξ . Additionally, we wish to consider the effect of using a cutoff regulator, which potentially violates the translation invariance of the theory. The photon self energy diagram, Fig. 1, treats both the fermion propagators in a symmetric way, but this symmetry will potentially not be respected by the cutoff regulator [29, 51, 83]; this is investigated numerically below by introducing a fermion loop variable parameter η with $k - \eta q$ the upper loop momentum in Fig. 1 and $k + (1 - \eta)q$ the lower. Two cases were investigated:

- $\eta = 1$ (the *asymmetric partition*) corresponds to loop momenta $k - q$ and k
- $\eta = 1/2$ (the *symmetric partition*) corresponds to loop momenta $k - q/2$ and $k + q/2$

In Fig. 4, we show the results of the fermion wavefunction renormalization and the corresponding effective (running) coupling versus momentum-squared for four gauges, $\xi = 0, 1, 2, 3$, and $\eta = 1/2$ with the modified Curtis-Pennington vertex (left panels) and Kızılersü-Pennington vertex (right panels). For both vertices the function F is dependent upon the gauge, as it must be; the solutions are virtually identical. However one sees the photon dressing function is strongly gauge dependent for the CP vertex, motivating the development of a ‘better’ vertex, the KP vertex, for which the improvement in the effective (running) coupling is instantly apparent. The solutions for four different choices of the gauge parameter lie almost on top of one another. The requirement that the vertex Ansatz ensures the DSE should be multiplicatively renormalizable dramatically reduces the violation of gauge invariance.

Figure 5 shows similar results as in Fig. 4 for the KP vertex, but with the asymmetric momentum partition $\eta = 1$. The difference between the two momentum partition schemes is most apparent in the running coupling in the infrared.

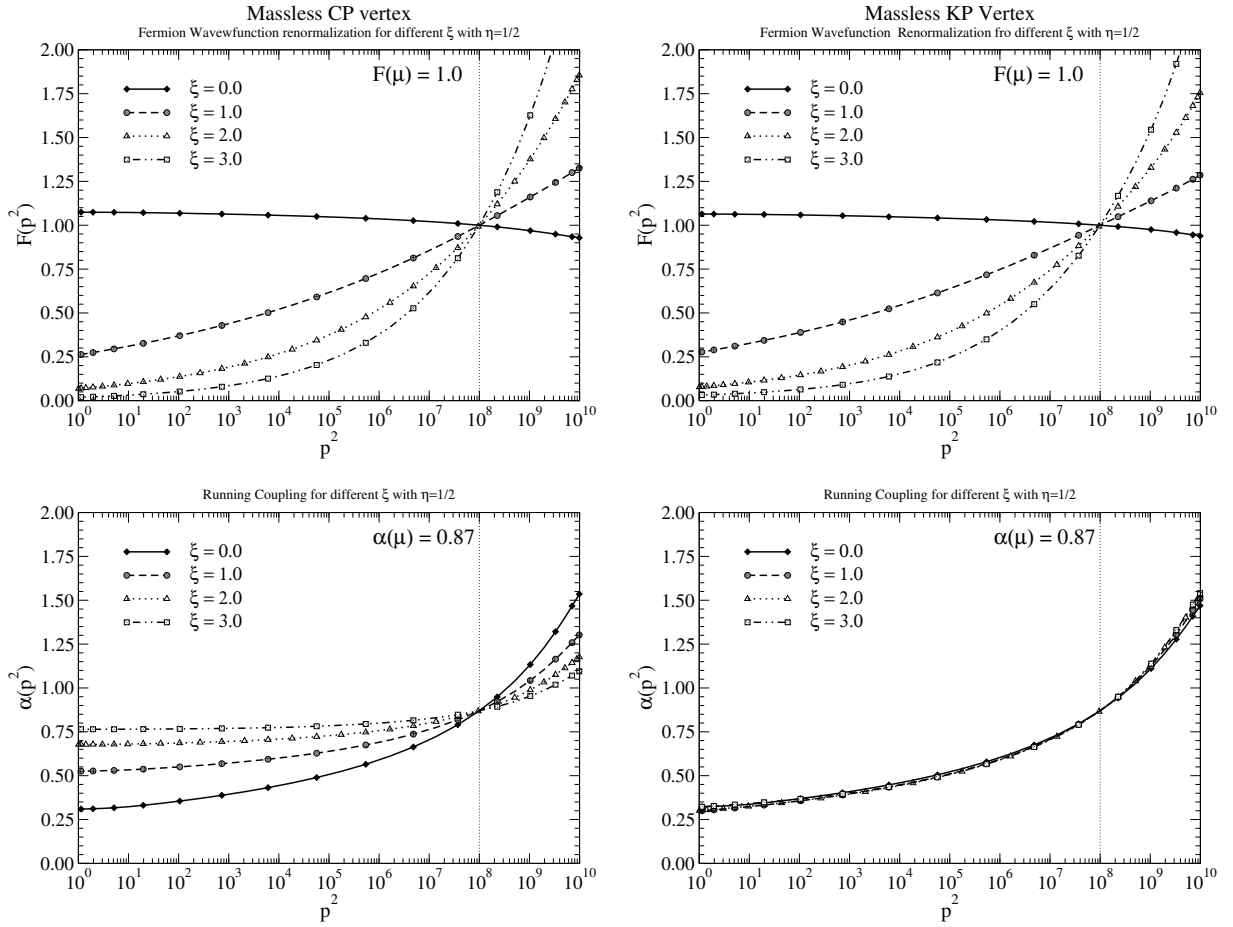


FIG. 4. Fermion wave-function renormalization and running coupling for $\xi = 0, 1, 2, 3$ and $\eta = 1/2$ (symmetric momenta partition) employing the Curtis–Pennington vertex (left) and Kızılersü–Pennington (right).

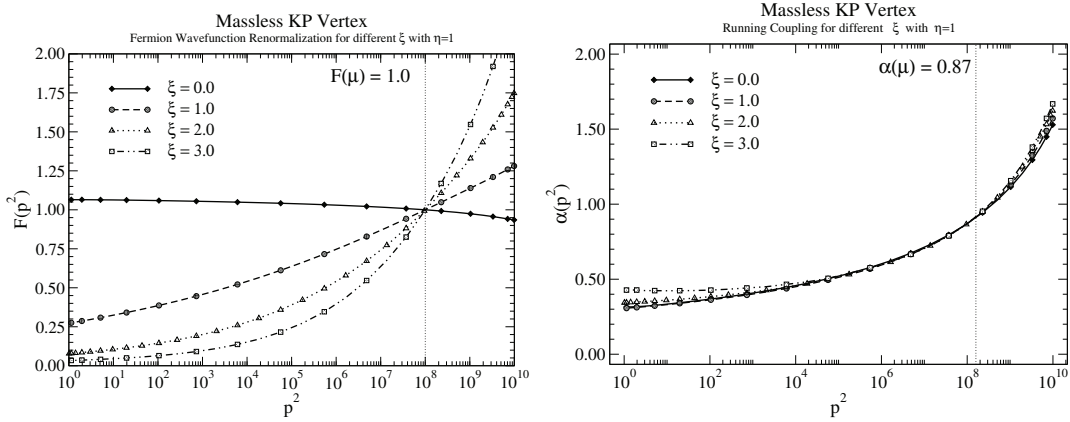


FIG. 5. Fermion wave-function renormalization and running coupling for $\xi = 0, 1, 2, 3$ and $\eta = 1$ (asymmetric momenta partition) employing the Kızılersü–Pennington vertex.

VI. MASSIVE UNQUENCHED QED₄ AND DYNAMICAL MASS GENERATION

A. Previous Studies

While exploring fermion mass generation in the unquenched (full) theory is the ultimate goal, historically

most effort devoted to this subject using the DSE formalism has been conducted using various approximations which make the system tractable : for example, the bare vertex and/or the quenched approximation. Fundamentally the aim of unquenching QED is to understand the

TABLE III. Critical couplings in the literature for different vertex Ansätze for in Landau gauge in unquenched QED₄. This is an extension to Table 4.1 in Ref. [28]

Ref.	$\alpha_c(N_F = 1)$	Vertex Model
[42]	1.9997 ($\xi = 0$)	Bare
[40]	1.95 ($\xi = 0$)	Bare
[45]	1.9989 ($\xi = 0$)	Bare
[45]	2.0728 ($\xi = 0$)	Bare
[46]	1.9995 ($\xi = 0$)	Bare
[92]	2.25 ($\xi = 0$)	Bare
[20]	2.10028 ($\xi = 0$)	Bare
[48]	2.084 ($\xi = 0$)	Bare
[47]	2.0944	NA
[93]	1.9995	NA
[28]	1.99953 ($\xi = 0$)	Bare
[28]	1.74102 @ $\Lambda^2(\xi = 0)$	Bare
[28]	1.63218 @ $\Lambda^2(\xi = 0)$	Ball-Chiu
[28]	1.61988 @ $\Lambda^2(\xi = 0)$	modified CP
[31]	2.27(Anal.), 2.4590(Num.) ($\xi = 0$)	BC+KP+A
[50]	0.9553 ($\xi = 0$)	BC+Ansatz

effects of the fermion loops on the interaction, namely the behaviour of the running coupling for a given physical system. There exists a large body of literature on dynamical fermion mass generation in unquenched QED₄ [27–29, 40–51] for various gauges ξ and number of flavours N_F . For reasons explained above, these necessarily involve truncations in the vertex and/or propagators; the most popular truncations are to replace the full photon wave function renormalization with its 1-loop perturbative expression, avoiding angular integrations in the DSEs, and solving the DSEs by iteration for F , M and G with the bare vertex. Invariably, cutoff regularization is used. The results obtained are qualitatively similar to the quenched case; namely, a phase transition occurs at some critical value of the coupling whereby fermion masses are generated dynamically; and (more controversially) the equations obey scaling laws from which conclusions are drawn regarding the continuum limit of the theory.

Some of these critical value studies in the literature are tabulated in Table III. Lattice studies also obtain dynamical mass generation and mass function scaling [81, 82, 84–91], but are not currently directly comparable because as explained above, they naturally contain a four-fermion interaction term.

B. Preliminaries

In this investigation, we use the two vertex Ansätze introduced in Section III: the Curtis–Pennington (CP) vertex and the Kızılersü–Pennington (KP) vertex. However, we cannot use the former directly in massive studies since the transverse component of the CP vertex given in Eq. (19) leads to a quadratic divergence in the photon DSE, due to the DSEs probing different kinematical re-

gions in the vertex [57]. Instead, we use two models (we call them models since they are clearly unrealistic, but serve to illuminate possible paths forward) where the CP vertex is used in the fermion DSE, and

- the Ball-Chiu construction without a transverse part is used in the photon DSE [28, 51] (the *modified CP vertex*)
- the KP vertex is used in the photon DSE [29] (the *modified KP vertex* or hybrid CP/KP vertex)

We also use cutoff regularization which should be recognized as an approximation, although there are doubts whether QED makes sense without one. We now proceed to investigate the consequences of the choice of the vertex on dynamical mass generation, and the gauge invariance of the consequent critical coupling. To accomplish this we introduce a sufficiently large coupling into the theory such that our solutions exhibit dynamical mass generation in the absence of a bare mass, for a selection of choices of the gauge parameter. The coupling strength is then decreased, in turn reducing the amount of mass generation, until we cross into the phase where only a massless solution exists. We use a renormalized formalism previously introduced in [25, 26], but constrained to solutions with zero bare mass ($m_0 = 0$). In this case, the mass function Eq. (A6) simplifies to

$$M(k^2) = \frac{\bar{\Sigma}_s(k^2)}{1 - \bar{\Sigma}_d(k^2)}. \quad (23)$$

In this section, all solutions have $\mu^2 = 10^8$ and $\Lambda^2 = 10^{10}$.

Typical fermion and photon propagator solutions for $m_0 = 0$ and fixed α_μ above criticality are presented in Fig. 6 (top) for three different gauges ($\xi_\mu = 0, 0.5, 1$). In Eq. (23) and Fig. 6 (top), $A(p^2)$ and $G(p^2)$ are renormalized solutions; however their unrenormalized counterparts can easily be calculated, as they are proportional to the renormalized solutions. Using Eqs. (4) and (5) we get

$$A_0(p^2, \Lambda^2) = A(p^2, \mu^2) / Z_2(\Lambda^2, \mu^2), \quad (24)$$

$$G_0(p^2, \Lambda^2) = G(p^2, \mu^2) Z_3(\Lambda^2, \mu^2), \quad (25)$$

the constants of proportionality are the fermion and photon renormalization constants, Z_2 and Z_3 respectively. As the coupling constant transforms oppositely to G , Eq. (12), the unrenormalized coupling is

$$\alpha_0 = \alpha / Z_3, \quad (26)$$

so that the *effective coupling* function

$$\alpha_{\text{eff}}(p^2) = \alpha(\mu^2) G(p^2, \mu^2) = \alpha_0(\Lambda^2) G_0(p^2, \Lambda^2), \quad (27)$$

is invariant. The mass function is similarly invariant, likewise $\alpha \xi$ is also an invariant quantity, so that ξ transforms like G , and will also be shifted in the unrenormalized solutions (except for Landau gauge). The unrenormalized solutions corresponding to the top panel of Fig. 6

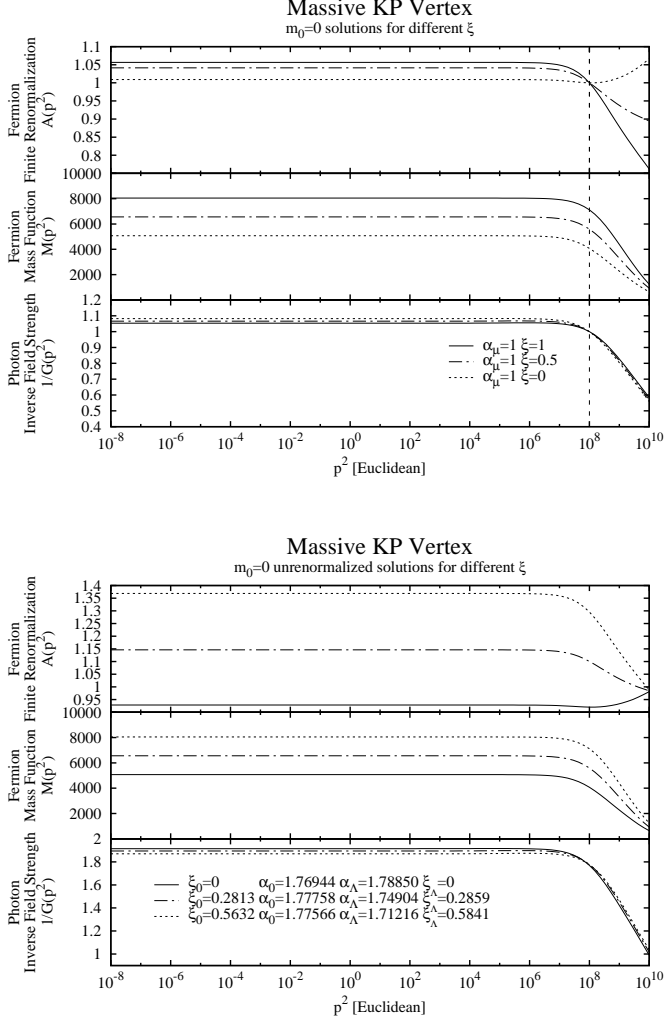


FIG. 6. Renormalized $m_0 = 0$ solutions for $\alpha_\mu = 1$, $\xi_\mu = 0, 0.5, 1$ (top) and corresponding unrenormalized solutions (bottom) for asymmetric momentum split ($\eta = 1$)

are presented in the bottom panel. Also displayed are

$$\alpha_\Lambda = \alpha_{\text{eff}}(\Lambda^2) = \alpha G(\Lambda^2) \quad \text{and} \quad \xi_\Lambda = \xi/G(\Lambda^2), \quad (28)$$

which are the parameters we would use for α and ξ if we wished to obtain the same solution as in Fig. 6, but renormalized at the cutoff (an example of a renormalization point transformation). Note that $\alpha_0 \approx \alpha_\Lambda$, and also $A(\Lambda^2) \approx 1$ and $G(\Lambda^2) \approx 1$: that is to say, the unrenormalized solutions are almost the same (but *not* identical) as solutions renormalized at the cutoff.

We also note that the unrenormalized solutions will scale with the cutoff according to their mass dimension: that is to say, under

$$\Lambda \rightarrow \Lambda', \quad (29)$$

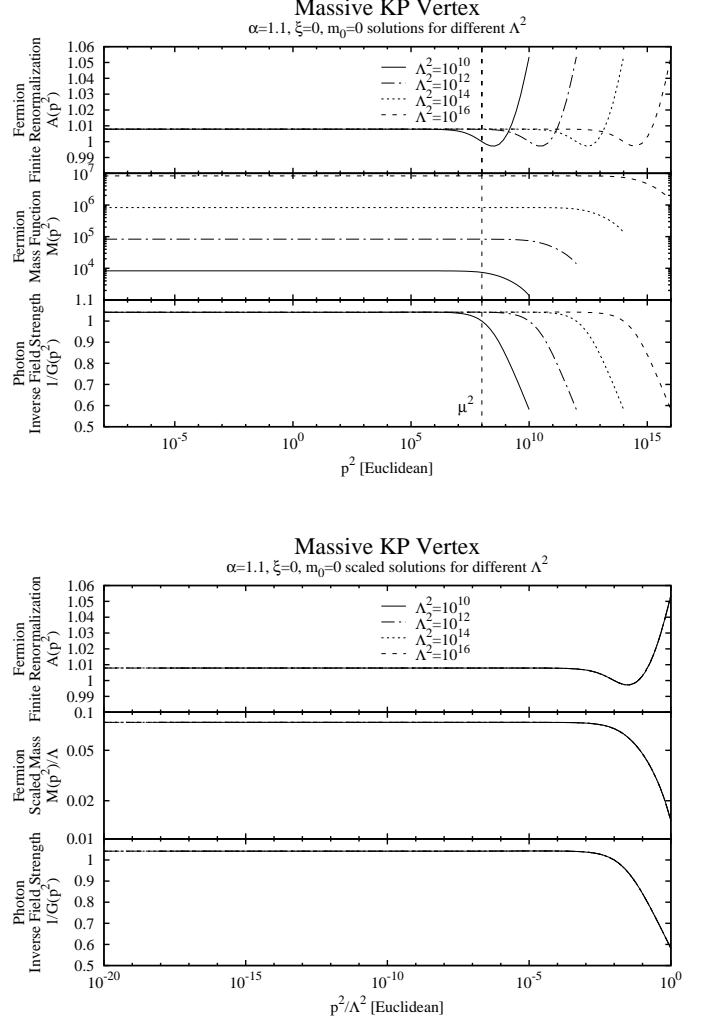


FIG. 7. $m_0 = 0$ solutions for $\alpha_\mu = 1.1$ and $\xi = 0$, scaling Λ^2 and μ^2 (top) and corresponding cutoff-relative solutions (bottom)

A_0 and G_0 as functions of p^2/Λ^2 are unchanged (as is α_0) and

$$M_0 \rightarrow \sqrt{\Lambda'/\Lambda} M_0. \quad (30)$$

These relations can only be maintained using the renormalized solutions if the renormalization point is scaled with the cutoff. Figure 7 illustrates the point [23]. When all mass scales, here Λ^2 and μ^2 (since $m_0 = 0$) are scaled simultaneously, the results are invariant when all momenta are plotted relative to the cutoff.

In the top Fig. 7 it is evident that, for zero bare mass solutions, the mass function scales with the cutoff. Furthermore, there is a general shift rightwards in momentum scale in all propagator functions, in proportion to the increase in cutoff. It behaves the same as the quenched theory, as studied in [94, 95]. In these papers, it was argued that this was evidence that QED did not have a

chiral limit in the usual sense. However, since the bare mass naturally varies with the cutoff, we should not expect bare mass solutions to be invariant against changes in the cutoff; rather the invariant solutions are the *scaled* solutions, as presented in the bottom Fig. 7.

These preliminary considerations show that it is viable to use a renormalized formalism to conduct a search for a critical coupling, below which the only solutions with $m_0 = 0$ are massless, provided we quote the unrenormalized coupling or the coupling at the cutoff in our results. Comparison with renormalized solutions is only possible without conversion if they have the same cutoff *and* renormalization point, or at least the same *ratio*. We also note the (inconvenient) shift in ξ for $\xi \neq 0$: this will vary with α .

C. Numerical Results

Figs. 8 and 9 illustrate the process for a symmetric momentum partition ($\eta = 1/2$). Each solution obtained at $\mu^2 = 10^8$ for the hybrid CP/KP vertex in Fig. 8 corresponds to an (α_Λ, m_E) point in (the bottom) Fig. 9, where $\alpha_\Lambda = \alpha_{eff}(\Lambda^2)$ and m_E is the Euclidean mass, derived from the mass function by the constraint

$$M(m_E^2) = m_E. \quad (31)$$

Here, and hereafter, solutions are renormalized at $\mu^2 = 10^8$ with $\Lambda^2 = 10^{10}$ and converged to one part in 10^5 or better at each momentum point.

The critical coupling α_c is extracted from the solutions in Fig. 9 by a least-squares fit of the form

$$m_E = \Lambda s (\alpha_\Lambda - \alpha_c)^p \quad (32)$$

where s , p and α_c are parameters to be fitted. Note that a simple power-law fit can be used, since the descent to criticality is much steeper than in the quenched case. Of course, the critical coupling at the renormalization point, or the unrenormalized critical coupling could be calculated instead, by fitting (α_μ, m_E) or (α_0, m_E) points. However, in all cases, the descent to criticality is along lines of constant ξ_μ .

It is admitted that the consequent shift in ξ explained in the previous section is a disadvantage to this method. However, in practice the shift is small (e.g. for KP $\xi = 1$, the shift is $\approx 1.7\%$) and decreases to insignificance as $\alpha \rightarrow \alpha_c$ reflecting the sharpness of the fall to criticality.

Figs. 10 and 11 show results for the asymmetric momenta split ($\eta = 1$), but for α_μ ; the results for α_Λ are shown in Fig. 12 which compares vertex Ansätze in the Landau (top figure) and Feynman (bottom figure) gauges. The outcomes for the Landau and Feynman gauges in both momentum partitioning schemes are summarized in Table IV: we adopt the expedient of truncating the shifted α_Λ and ξ_Λ results to four and two decimal places respectively.

We note that there is a small but significant variation in the results for the different momentum partitioning. We further note that in all cases, and using either momentum partitioning scheme, the hybrid CP/KP vertex exhibits the least gauge variance. Also, for α_c calculated at the cutoff, the modified CP and KP vertices give very similar results in either momentum partitioning scheme for both Landau and Feynman gauges, although there is a wide gauge variation. However, remarkably, the results for α_c at the renormalization point differ widely for the modified CP and KP vertices.

It is evident that despite the successes of the KP vertex in the massless limit, where the breaking of gauge-invariance was significantly suppressed by the satisfying of multiplicative renormalizability, it is not as good in this regard as the hybrid CP/BC vertex when dynamical mass generation is manifest. Presumably, the reason for this is that the KP vertex does not yet include any mass terms in it, i.e. the transverse form factors $\tau_{1,4,5,7}$ in the transverse vertex, Eq. (15), have been chosen to vanish. We envisage that this means that the leading and sub-leading logarithms in a perturbative expansion of the mass function are not correctly related.

D. Condensate

Another signal of dynamical mass generation is that the condensate

$$\langle 0 | \bar{\Psi} \Psi | 0 \rangle = -\frac{4}{\pi} \int dp^2 \frac{p^2 B(p^2)}{p^2 A^2(p^2) + B^2(p^2)}, \quad (33)$$

is non-zero if and only if we are above criticality. In Fig. 13, we show the condensates for the solutions in Fig. 11, as functions of $\alpha - \alpha_c$, and resultant fits which show power-law behaviour. Also notable is the condensates exhibit the same gauge-variant behaviour as the solutions in Fig. 11: that is, the hybrid CP/KP vertex solutions exhibit the least gauge variance, and the KP vertex the most.

E. Comparison With Other Studies

Ref. [28] uses the modified CP vertex in their unquenched QED₄ work where they solve the DSEs by iteration. They found the critical coupling $\alpha_c(\Lambda^2, N_F = 1) = 1.61988$ which agrees with our results $\alpha_c(\Lambda^2, N_F = 1) = 1.61567$ in Landau gauge very well. Bashir et.al [31] studied dynamical mass generation in Landau gauge using the KP vertex together with another additional transverse piece for various number of fermion flavours their result for the critical coupling $\alpha_c^A(N_F = 1) = 2.27$ (analytically and $\Lambda^2 \rightarrow \infty$ is taken) and $\alpha_c^N(\Lambda^2, N_F = 1) = 2.4590$ (numerically) and they found their analytical and numerical results on the dynamically generated mass function differs slightly. Both the solutions exhibits the scaling law, $M(0)/\Lambda^2 = a(\alpha - \alpha_c)^p$ with the exponent of

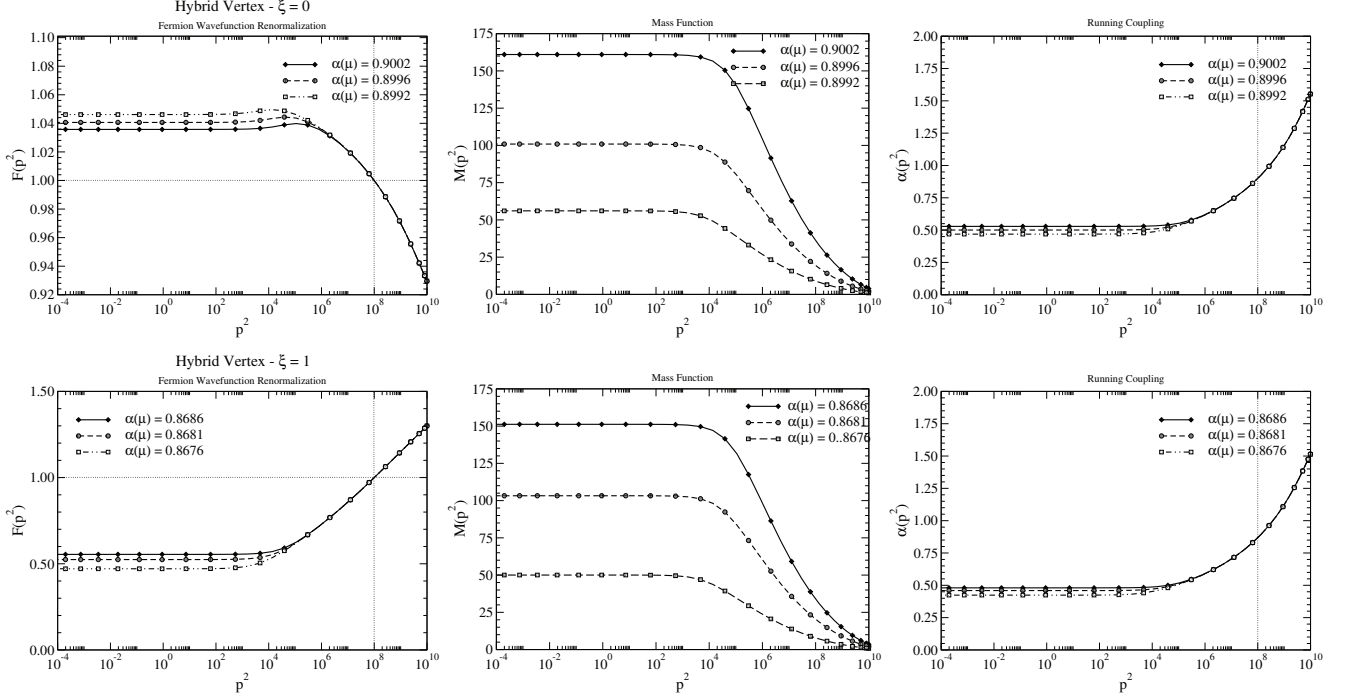


FIG. 8. Typical $m_0 = 0$ solutions in the Landau gauge (top plots) and Feynman gauge (bottom plots), using the unquenched CP/KP hybrid vertex, for a symmetric momentum partition ($\eta = 1/2$). Shown, from left to right, are the wave-function renormalization, mass and running coupling (effective alpha) functions.

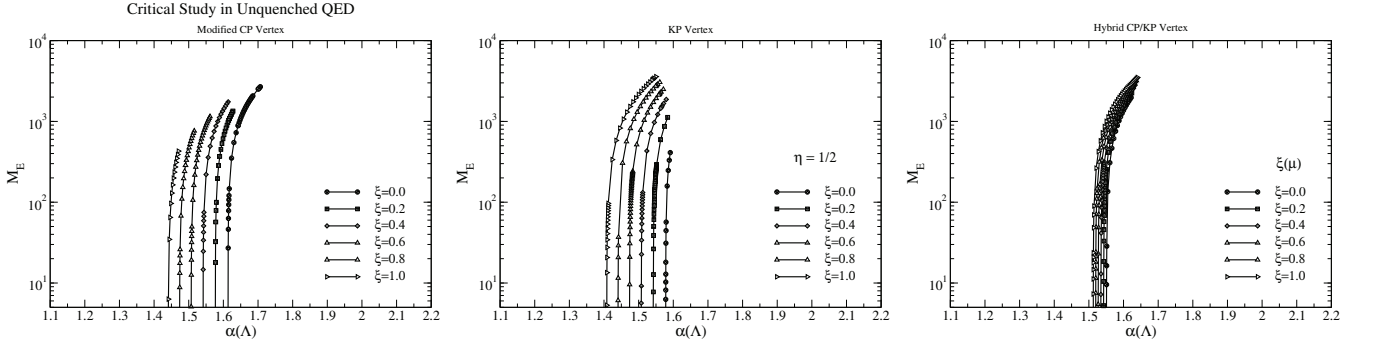


FIG. 9. Euclidean mass vs. coupling α_Λ for $m_0 = 0$ solutions for the modified CP (left), KP (middle) and hybrid CP/KP (right) vertex Ansätze for a spread of gauges and $\eta = 1/2$.

TABLE IV. Critical couplings at the renormalization point (α_μ), at the cut-off (α_Λ) and unrenormalized (α_0) for the Landau and Feynman gauges using the modified CP vertex, KP vertex and hybrid CP/KP vertex, for symmetric and asymmetric momentum partitions. Note that, except in Landau gauge, calculating α_Λ and α_0 necessitates a shift in ξ as well. These results were generated by the Durham group [29]. The asymmetric results were also generated by the Adelaide group independently and found to be in agreement.

		Symmetric ($\eta = 1/2$)			Asymmetric ($\eta = 1$)				
Vertex	ξ_μ	α_μ	ξ_Λ	α_Λ	α_μ	ξ_Λ	α_Λ	ξ_0	α_0
Mod. CP	0	0.87127	0.00	1.6135	0.87158	0.00	1.6152	0.00	1.6001
Mod. CP	1	0.90681	0.63	1.4409	0.90921	0.63	1.4358	0.62	1.4749
KP	0	0.90567	0.00	1.5783	0.89632	0.00	1.6158	0.00	1.5989
KP	1	0.83658	0.59	1.4080	0.82895	0.58	1.4361	0.56	1.4766
Hybrid KP	0	0.89860	0.00	1.5504	0.88926	0.00	1.5873	0.00	1.5701
Hybrid KP	1	0.86726	0.57	1.5126	0.85935	0.56	1.5449	0.54	1.5944

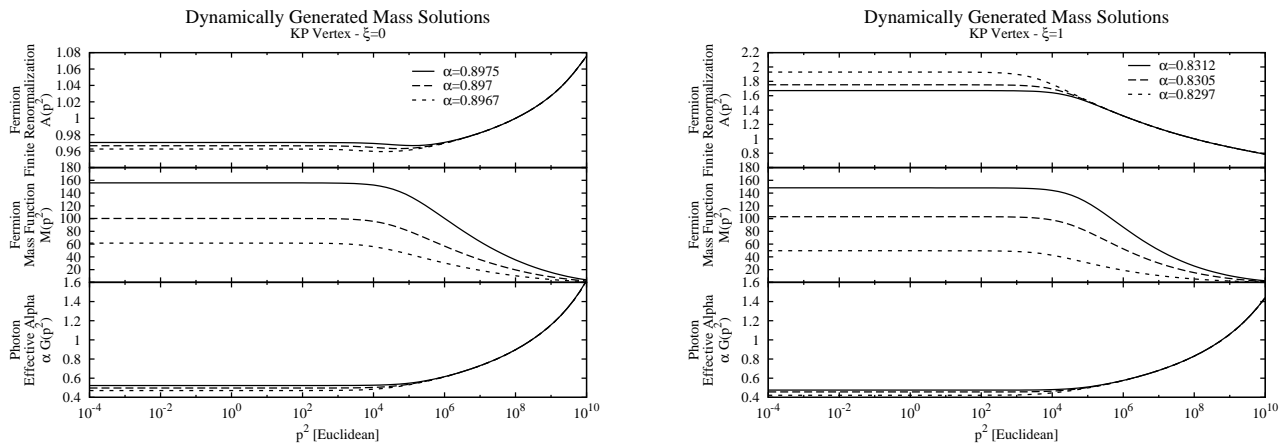


FIG. 10. Inverse wave-function renormalization, mass-function and running coupling in Landau (left) and Feynman (right) gauges using the KP vertex in asymmetric momentum partition.

$p = 0.5$ (analytically), $p = 0.7819$ (numerically). Our critical value for $N_F = 1$ is much smaller than theirs but our exponent of the power law $p = 0.89631$ is larger than theirs. Referring again to Fig. 8 for comparison, we chose values such that the resulting masses $M(0)$ were approximately equivalent. Clearly, the wave-functions show their intrinsic gauge variance. This is present also in the mass-functions, but is masked somewhat by the generation of a mass and is mainly discernible from differences in the ultraviolet behaviour. The key test, however, is in the dressing functions for the photon propagator which should be invariant under a change of gauge. We see that the solutions for two gauges are in fact very similar – as is most evident from the plots of Fig. 11.

VII. CONCLUSION AND FUTURE WORK

In this article we studied dynamical mass generation in unquenched QED₄ by solving the DSEs for the fermion and photon propagators. Given a suitable Ansatz for the fermion-photon vertex, the infinite tower of equations can be truncated, forming a closed system of coupled non-linear integral equations that are solved numerically by iteration.

In the absence of any explicit mass term in the Lagrangian, fermions remain massless until the gauge coupling reaches some critical value whereupon the fermions acquire a dynamical mass. This occurs in both quenched QED (where the coupling does not run and the photon propagator is trivial) and unquenched QED. The value of the critical point depends on the choice of vertex adopted to solve these equations. Ideally, the photon propagator and critical coupling should be independent of the choice of gauge: its actual degree of gauge variance is an important constraint for constructing a fermion-photon vertex as well as a test for checking the quality of the truncation introduced. While the bare vertex leads to

a highly gauge dependent critical coupling, the CP and KP vertices perform much better in this regard due to their construction. Recall the CP vertex was constructed to make the fermion propagator consistent with multiplicative renormalizability. Since this represents a kinematic region in which a large momentum flows through a fermion line to the photon leaving the other fermion with fixed momentum, it fails in the photon equation when ultra-violet renormalization concerns large momenta in the fermion legs, with the photon momentum fixed. Consequently, the CP vertex, widely used in quenched studies, is incompatible with unquenched QED, except in the massless case. In contrast, the KP vertex aims to make both the fermion and photon propagator equations consistent with multiplicative renormalizability in the case of massless fermions.

The main aim of this paper has been to explore the performance of the KP vertex with regard to gauge invariance when a dynamical mass is generated. This analysis has highlighted the sensitivity to the fact that the design of the KP vertex is incomplete, since no mass terms are included in its structure. Hence, for comparison purposes, two hybrid vertices were also considered: these used the CP vertex for the fermion equation, and the Ball-Chiu and the KP vertex respectively for the photon equation. It was found that the latter vertex (the hybrid CP/KP vertex) exhibited the least gauge variance. Another possible source of gauge variance is the use of a cutoff regulator: by employing two different schemes for evaluating the fermion loop momenta, it was found that this effect was also non-trivial. This illustrates how our understanding of strong coupling QED is as yet incomplete, and in need of further study.

As soon as fermion loops are introduced in the QED vacuum, the electric charge is screened and the effective coupling starts to run. One of the outstanding questions in full QED is how much screening the effective running coupling will receive in the continuum limit ($\Lambda \rightarrow \infty$)?

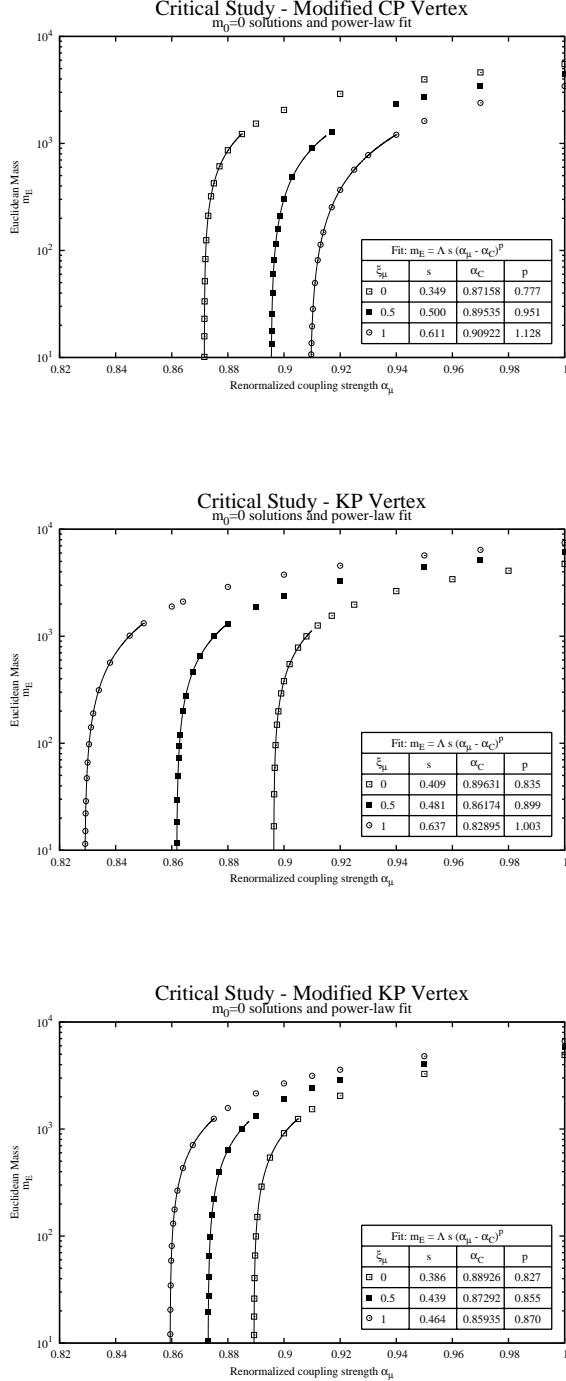


FIG. 11. Euclidean mass vs. coupling α_μ for $m_0 = 0$ solutions for the modified CP (top), KP (middle) and hybrid CP/KP (bottom) vertex Ansätze for $\xi_\mu = 0, 0.5, 1$, $\eta = 1$ and corresponding power-law fits in asymmetric momentum partition.

Will the effective running coupling die off and the theory become free and non-interacting? Or at large momenta does the coupling become so big that new operators, like

that of four-fermions, become relevant in such a way that the theory remains interacting, and non-trivial. Answering these questions is outside the scope of this paper, but the subject of subsequent work to be reported elsewhere. There the relevant operators will be added to the Lagrangian allowing their effect to be quantified.

ACKNOWLEDGMENTS

We would also like to thank C. S. Fischer and C. D. Roberts for useful discussions. AK and TS thank A. W. Thomas for supporting this study under the aegis of the Centre for the Subatomic Study of Matter (CSSM). We also acknowledge support from the Australian Research Council International Linkage Award (LX 0776452), the Australian Research Council Discovery grant (DP0558878), and the Austrian Science Fund (FWF) under project number M1333-N16. MRP acknowledges support of Jefferson Science Associates, LLC under U.S. DOE Contract No. DE-AC05-06OR23177 for the writing of this paper.

Appendix A: Dyson–Schwinger equations (DSEs)

The fermion and the photon Dyson–Schwinger equations which are solved iteratively for the fermion and photon wave function renormalizations and for the mass function are given below.

1. Fermion Wave-function Renormalization

The fermion self-energy in Eq. (1) can be decomposed into Dirac and scalar terms, $\bar{\Sigma}(p) = \bar{\Sigma}_d(p) \not{p} + \bar{\Sigma}_s(p)$ which is obtained from $\Sigma(p)$ by

$$\bar{\Sigma}_d(p^2) = \frac{1}{4} \text{Tr} \left(\bar{\Sigma}(p) \frac{\not{p}}{p^2} \right), \quad \bar{\Sigma}_s(p^2) = \frac{1}{4} \text{Tr} (\bar{\Sigma}(p) \cdot \mathbb{1}). \quad (\text{A1})$$

Multiplying Eq. (1) by \not{p} and $\mathbb{1}$ respectively yields two separate equations for the inverse fermion wave-function renormalization and the mass function :

$$F^{-1}(\mu^2; p^2) = Z_2(\mu) - Z_2(\mu) \bar{\Sigma}_d(p^2), \quad (\text{A2})$$

$$M(p^2) F^{-1}(\mu^2; p^2) = Z_2(\mu) m_0 + Z_2(\mu) \bar{\Sigma}_s(p^2). \quad (\text{A3})$$

Evaluating Eqs. (A2,A3) at the renormalization point, $p^2 = \mu^2$, and forming an appropriate difference one can eliminate the divergent constants Z_1 and Z_2 to obtain the renormalized quantities

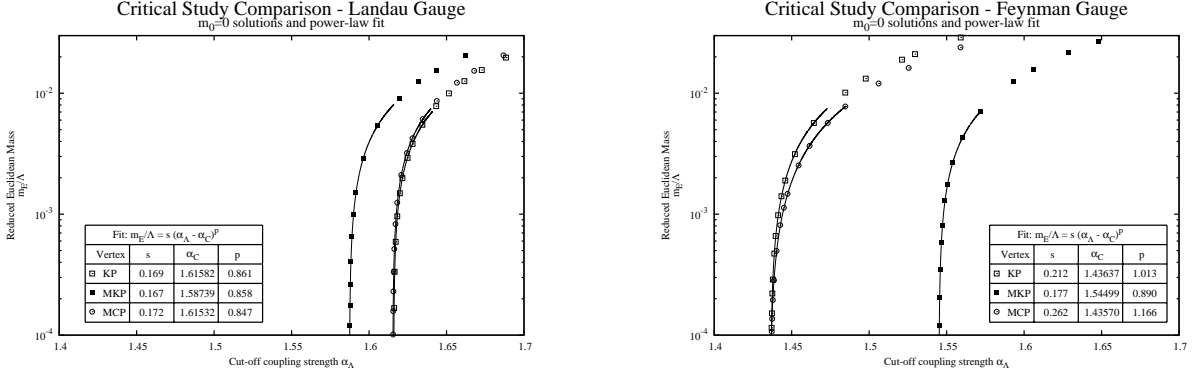


FIG. 12. Vertex comparison of dynamically generated mass, $m_0 = 0$, solutions coupling at the cutoff, for the Landau (left) and Feynman (right) gauges and $\eta = 1$.

$$F(\mu^2; p^2) = 1 + F(\mu^2; p^2) \bar{\Sigma}_d(p^2) - \bar{\Sigma}_d(\mu^2), \quad (\text{A4})$$

$$\begin{aligned} \bar{\Sigma}_d(p^2) = & \frac{\alpha}{4\pi^3} \int_E d^4k \frac{1}{p^2} \frac{1}{q^2} \frac{F_k}{[k^2 + M_k^2]} \left[-\frac{\xi}{q^2} \frac{1}{F_p} [p^2 k \cdot q + M_k M_p p \cdot q] \right. \\ & + \frac{G_q}{q^2} \left\{ \frac{1}{2} \left(\frac{1}{F_k} + \frac{1}{F_p} \right) [-2\Delta^2 - 3q^2 k \cdot p] + \frac{1}{2(k^2 - p^2)} \left(\frac{1}{F_k} - \frac{1}{F_p} \right) [-2\Delta^2(k^2 + p^2)] \right. \\ & \left. \left. + \frac{1}{(k^2 - p^2)} \left(\frac{M_k^2}{F_k} - \frac{M_p M_k}{F_p} \right) [-2\Delta^2] \right\} \right. \\ & \left. + G_q \left\{ \tau_2^E(p^2, k^2, q^2) [-\Delta^2(k^2 + p^2)] + \tau_3^E(p^2, k^2, q^2) [2\Delta^2 + 3q^2 k \cdot p] \right. \right. \\ & \left. \left. + \tau_6^E(p^2, k^2, q^2) [3k \cdot p(p^2 - k^2)] + \tau_8^E(p^2, k^2, q^2) M_k [-2\Delta^2] \right\} \right], \quad (\text{A5}) \end{aligned}$$

where $\Delta^2 = (k \cdot p)^2 - k^2 p^2$ and

$$M(p^2) = m_\mu + [M(p^2) \bar{\Sigma}_d(p^2) + \bar{\Sigma}_s(p^2)] - [m_\mu \bar{\Sigma}_d(\mu^2) + \bar{\Sigma}_s(\mu^2)], \quad (\text{A6})$$

$$\begin{aligned} \bar{\Sigma}_s(p) = & \frac{\alpha}{4\pi^3} \int_E d^4k \frac{1}{q^2} \frac{F_k}{[k^2 + M_k^2]} \left[\frac{\xi}{q^2} \frac{1}{F_p} [k \cdot q M_p - p \cdot q M_k] \right. \\ & + G_q \left\{ \frac{1}{2} \left[\frac{1}{F_k} + \frac{1}{F_p} \right] M_k [3] + \frac{1}{2(k^2 - p^2)} \left[\frac{1}{F_k} - \frac{1}{F_p} \right] M_k \left[\frac{-4\Delta^2}{q^2} \right] + \frac{1}{(k^2 - p^2)} \left[\frac{M_k}{F_k} - \frac{M_p}{F_p} \right] \left[\frac{2\Delta^2}{q^2} \right] \right\} \\ & \left. + G_q \left\{ \tau_2^E(p^2, k^2, q^2) [-2\Delta^2] M_k + \tau_3^E(p^2, k^2, q^2) [-3q^2] M_k + \tau_6^E(p^2, k^2, q^2) [-3(p^2 - k^2)] M_k \right\} \right]. \quad (\text{A7}) \end{aligned}$$

We have represented arguments by subscripts for brevity $F_k = F(k^2)$.

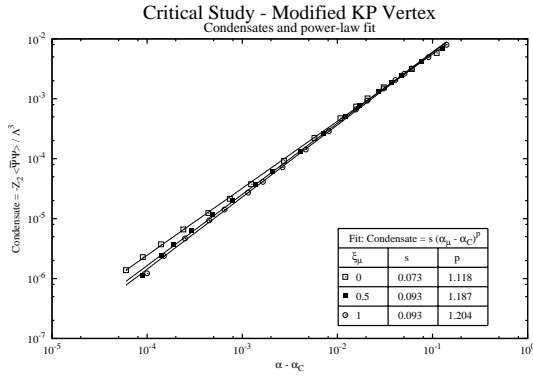
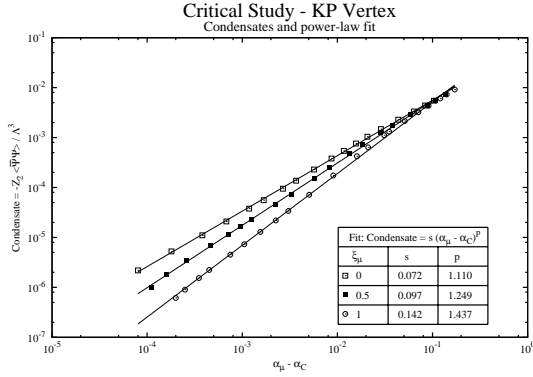
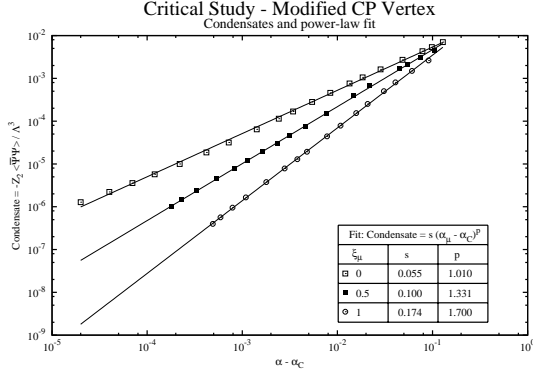


FIG. 13. A log-log plot of the condensate versus $\alpha - \alpha_c$ for $m_0 = 0$ using modified CP vertex (top), KP vertex (middle) and hybrid CP/KP vertex (bottom).

2. Photon Wave-function Renormalization

The renormalized photon DSE from Eq. (2) is

$$\Delta_{\mu\nu}^{-1}(q) = Z_3(\mu) (\Delta_{\mu\nu}^0)^{-1}(q) + Z_1(\mu) \bar{\Pi}_{\mu\nu}(q), \quad (\text{A8})$$

where $\bar{\Pi}_{\mu\nu}$ is the photon vacuum polarization or self-energy obtained by evaluating the photon DSE diagram using the Feynman rules.

If we contract the photon self-energy with q^μ :

$$q^\mu \bar{\Pi}_{\mu\nu}(q) = ie^2 N_F \text{Tr} \int_M \widetilde{dk} \gamma_\nu S(k) (q \cdot \Gamma(p, k)) S(p), \quad (\text{A9})$$

and use the WGTI

$$q^\mu \bar{\Pi}_{\mu\nu}(q) = ie^2 N_F \text{Tr} \int_M \widetilde{dk} \gamma_\nu (S(k) - S(p)), \quad (\text{A10})$$

where $\widetilde{dk} = d^4k/(2\pi)^4$ and $p = k - q$.

Using an analogous procedure to the fermion propagator, we can form the appropriate subtractions of the renormalized photon DSEs, Eq. (A8) to eliminate the divergent renormalization constants Z_1 and Z_3 by recalling that $G(\mu^2; \mu^2) = 1$ yields :

$$G^{-1}(\mu^2; q^2) = 1 + [G^{-1}(\mu^2; q^2) \bar{\Sigma}_d(\mu^2) + \bar{\Pi}(q^2)] - [\bar{\Sigma}_d(\mu^2) + \bar{\Pi}(\mu^2)], \quad (\text{A11})$$

$$\bar{\Pi}(q^2) = \frac{\alpha N_F}{3\pi^3} \int_E d^4k \frac{1}{q^2} \frac{F_p}{(p^2 + M_p^2)} \frac{F_k}{(k^2 + M_k^2)} \left\{ \frac{1}{2} \left(\frac{1}{F_k} + \frac{1}{F_p} \right) \left[2k \cdot p - \frac{8}{q^2} (\Delta^2 + q^2 k \cdot p) \right] \right\}$$

$$\begin{aligned}
& + \frac{1}{2} \frac{(1/F_k - 1/F_p)}{(k^2 - p^2)} \left[-(k^2 + p^2) + 2M_k M_p \left\{ \frac{8}{q^2} (k \cdot q)^2 - 3k \cdot q - 2k^2 \right\} - 3(k^2 - p^2) (M_k M_p - k^2) \right] \\
& + \frac{(M_k/F_k - M_p/F_p)}{k^2 - p^2} \left[-(M_k + M_p) \left\{ \frac{8}{q^2} (k \cdot q)^2 - 3k \cdot q - 2k^2 \right\} + 3(k^2 - p^2) M_k \right], \\
& + \tau_2^E(p^2, k^2, q^2) [(k^2 + p^2) \{-\Delta^2\} + M_k M_p \{2\Delta^2\}] + \tau_3^E(p^2, k^2, q^2) [3q^2 k \cdot p + 2\Delta^2 + M_k M_p \{3q^2\}] \\
& + \tau_6^E(p^2, k^2, q^2) [3k \cdot p (p^2 - k^2) + M_k M_p \{3(p^2 - k^2)\}] + \tau_8^E(p^2, k^2, q^2) [-2\Delta^2] \Big\}. \quad (A12)
\end{aligned}$$

-
- [1] R. Alkofer, C. S. Fischer, F. J. Llanes-Estrada, and K. Schwenzer, *Annals Phys.* **324**, 106 (2009).
- [2] R. Williams, (2014), [arXiv:hep-ph/1404.2545 \[hep-ph\]](#).
- [3] A. Aguilar, D. Binosi, D. Ibaez, and J. Papavassiliou, (2014), [arXiv:1405.3506 \[hep-ph\]](#).
- [4] A. Aguilar, D. Binosi, D. Ibaez, and J. Papavassiliou, *Phys. Rev.* **D89**, 085008 (2014).
- [5] A. Blum, M. Q. Huber, M. Mitter, and L. von Smekal, *Phys. Rev.* **D89**, 061703 (2014).
- [6] G. Eichmann, R. Williams, R. Alkofer, and M. Vujanovic, *Phys. Rev.* **D89**, 105014 (2014).
- [7] V. Gusynin and M. Reenders, *Phys. Rev.* **D68**, 025017 (2003).
- [8] T. Goecke, C. S. Fischer, and R. Williams, *Phys. Rev.* **B79**, 064513 (2009).
- [9] M. Franz, Z. Tسانovic, and O. Vafek, *Phys. Rev.* **B66**, 054535 (2002).
- [10] Z. Tسانovic, O. Vafek, and M. Franz, *Phys. Rev.* **B65**, 180511 (2002).
- [11] J. A. Bonnet, C. S. Fischer, and R. Williams, *Phys. Rev.* **B84**, 024520 (2011).
- [12] P. Fomin and V. Miransky, *Phys. Lett.* **B64**, 166 (1976).
- [13] V. Miransky, *Nuovo Cim.* **A90**, 149 (1985).
- [14] V. Miransky, *Sov. Phys. JETP* **61**, 905 (1985).
- [15] V. Miransky, *Phys. Lett.* **B165**, 401 (1985).
- [16] V. Miransky, *Phys. Lett.* **B91**, 421 (1980).
- [17] R. Fukuda and T. Kugo, *Nucl. Phys.* **B117**, 250 (1976).
- [18] P. Fomin, V. Gusynin, V. Miransky, and Y. Sitenko, *Riv. Nuovo Cim.* **6N5**, 1 (1983).
- [19] M. Lombardo, A. Kocic, and J. Kogut, *Nucl. Phys. Proc. Suppl.* **42**, 687 (1995).
- [20] D. Atkinson, H. de Groot, and P. Johnson, *Int. J. Mod. Phys.* **A7**, 7629 (1992).
- [21] D. Atkinson and P. Johnson, *Phys. Rev.* **D35**, 1943 (1987).
- [22] D. Atkinson, J. C. Bloch, V. Gusynin, M. Pennington, and M. Reenders, *Phys. Lett.* **B329**, 117 (1994).
- [23] D. Curtis and M. Pennington, *Phys. Rev.* **D48**, 4933 (1993).
- [24] D. Curtis and M. Pennington, *Phys. Rev.* **D46**, 2663 (1992).
- [25] A. Kizilersu, A. W. Schreiber, and A. G. Williams, *Phys. Lett.* **B499**, 261 (2001).
- [26] A. Kizilersu, T. Sizer, and A. G. Williams, *Phys. Rev.* **D65**, 085020 (2002).
- [27] J. C. Bloch and M. Pennington, *Mod. Phys. Lett.* **A10**, 1225 (1995).
- [28] J. C. Bloch, (1995), [arXiv:hep-ph/0208074 \[hep-ph\]](#).
- [29] R. Williams, *Ph.D Thesis: Schwinger-Dyson equations in QED and QCD: The Calculation of fermion-antifermion condensates*, <http://etheses.dur.ac.uk/2558/> (Durham University, 2007).
- [30] A. Bashir and M. Pennington, *Phys. Rev.* **D50**, 7679 (1994).
- [31] A. Bashir, R. Bermudez, L. Chang, and C. Roberts, *Phys. Rev.* **C85**, 045205 (2012).
- [32] V. Gusynin, A. Schreiber, T. Sizer, and A. G. Williams, *Phys. Rev.* **D60**, 065007 (1999).
- [33] F. T. Hawes and A. G. Williams, *Phys. Lett.* **B268**, 271 (1991).
- [34] F. T. Hawes and A. G. Williams, *Phys. Rev.* **D51**, 3081 (1995).
- [35] F. T. Hawes, A. G. Williams, and C. D. Roberts, *Phys. Rev.* **D54**, 5361 (1996).
- [36] A. G. Williams and F. Hawes, *Nucl. Phys. Proc. Suppl.* **47**, 691 (1996).
- [37] M. Reenders, (1999), [arXiv:hep-th/9906034 \[hep-th\]](#).
- [38] P. Fomin, V. Gusynin, V. Miransky, and Y. Sitenko, (1984).
- [39] C. D. Roberts and A. G. Williams, *Prog. Part. Nucl. Phys.* **33**, 477 (1994).
- [40] V. Gusynin, *Mod. Phys. Lett.* **A5**, 133 (1990).
- [41] V. Gusynin and V. Kushnir, *Phys. Lett.* **B242**, 474 (1990).
- [42] K.-i. Kondo and H. Nakatani, *Nucl. Phys.* **B351**, 236 (1991).
- [43] K.-I. Kondo, *Nucl. Phys.* **B351**, 259 (1991).
- [44] K.-i. Kondo, *Int. J. Mod. Phys.* **A6**, 5447 (1991).
- [45] K.-i. Kondo and H. Nakatani, *Prog.Theor.Phys.* **88**, 737 (1992).
- [46] J. Oliensis and P. Johnson, *Phys. Rev.* **D42**, 656 (1990).
- [47] M. Ukita, M. Komachiya, and R. Fukuda, *Int. J. Mod. Phys.* **A5**, 1789 (1990).
- [48] K.-I. Kondo, H. Mino, and H. Nakatani, *Mod. Phys. Lett.* **A7**, 1509 (1992).
- [49] A. Bashir, C. Calcaneco-Roldan, L. Gutierrez-Guerrero, and M. Tejeda-Yeomans, *Phys. Rev.* **D83**, 033003 (2011).
- [50] F. Akram, A. Bashir, L. Gutierrez-Guerrero, B. Masud, J. Rodriguez-Quintero, *et al.*, *Phys. Rev.* **D87**, 013011 (2013).
- [51] A. Kizilersu, T. Sizer, and A. G. Williams,

- Phys. Rev. **D88**, 045008 (2013).
- [52] P. Maris and P. C. Tandy, Phys. Rev. **C61**, 045202 (2000).
- [53] C. Kellermann and C. S. Fischer, Phys. Rev. **D78**, 025015 (2008).
- [54] M. Q. Huber, A. Maas, and L. von Smekal, JHEP **1211**, 035 (2012).
- [55] E. Rojas, J. de Melo, B. El-Bennich, O. Oliveira, and T. Frederico, JHEP **1310**, 193 (2013).
- [56] T. Sizer, *Ph.D Thesis* (2013).
- [57] A. Kizilersu and M. Pennington, Phys. Rev. **D79**, 125020 (2009).
- [58] D. Curtis and M. Pennington, Phys. Rev. **D42**, 4165 (1990).
- [59] J. Ward, Phys. Rev. **78**, 182 (1950).
- [60] H. Green, Proc.Phys.Soc. **A66**, 873 (1953).
- [61] Y. Takahashi, Nuovo Cim. **6**, 371 (1957).
- [62] J. S. Ball and T.-W. Chiu, Phys. Rev. **D22**, 2542 (1980).
- [63] A. Kizilersu, M. Reenders, and M. Pennington, Phys. Rev. **D52**, 1242 (1995).
- [64] J. C. Collins, *Renormalization : an introduction to renormalization, the renormalization group, and the operator-product expansion*, Cambridge monographs on mathematical physics (Cambridge University Press, Cambridge [Cambridgeshire]; New York, 1984).
- [65] C. Itzykson and J. B. Zuber, *Quantum field theory*, International series in pure and applied physics (McGraw-Hill International Book Co., New York, 1980).
- [66] C. J. Burden and C. D. Roberts, Phys. Rev. **D47**, 5581 (1993).
- [67] T. D. C.S. Fischer, R. Alkofer and P. Maris, Phys. Rev **D70**, 073007 (2004).
- [68] C. Fischer and R. Alkofer, Phys. Rev **D67**, 094020 (2003).
- [69] C. F. R. Alkofer, W. Detmold and P. Maris, Phys. Rev **D70**, 014014 (2004).
- [70] A. W. Schreiber, T. Sizer, and A. G. Williams, Phys. Rev. **D58**, 125014 (1998).
- [71] D. Curtis, M. Pennington, and D. Walsh, Phys. Lett. **B249**, 528 (1990).
- [72] A. Bashir and M. Pennington, Phys. Rev. **D53**, 4694 (1996).
- [73] C. N. Leung, S. Love, and W. A. Bardeen, Nucl. Phys. **B323**, 493 (1989).
- [74] V. Miransky, T. Nonoyama, and K. Yamawaki, Mod. Phys. Lett. **A4**, 1409 (1989).
- [75] V. Gusynin and M. Reenders, Phys. Rev. **D57**, 6356 (1998).
- [76] K.-i. Kondo and H. Nakatani, Mod. Phys. Lett. **A4**, 2155 (1989).
- [77] K.-i. Kondo, H. Mino, and K. Yamawaki, Phys. Rev. **D39**, 2430 (1989).
- [78] J. Kogut and J. Lagae, Nucl. Phys. Proc. Suppl. **34**, 552 (1994).
- [79] J. Kogut and J. Lagae, Nucl. Phys. Proc. Suppl. **42**, 681 (1995).
- [80] J. B. Kogut, E. Dagotto, and A. Kocic, Nucl. Phys. **B317**, 253 (1989).
- [81] A. Kocic, S. Hands, J. B. Kogut, and E. Dagotto, Nucl. Phys. **B347**, 217 (1990).
- [82] A. Kocic, J. B. Kogut, M.-P. Lombardo, and K. Wang, Nucl. Phys. **B397**, 451 (1993).
- [83] A. Kizilersu, *Ph.D Thesis: Gauge Theory Constraints on the Fermion-Boson Vertex*, <http://etheses.dur.ac.uk/4886/> (Durham University, 1995).
- [84] K.-I. Aoki, M. Bando, T. Kugo, K. Hasebe, and H. Nakatani, Prog.Theor.Phys. **81**, 866 (1989).
- [85] E. Dagotto, J. B. Kogut, and A. Kocic, Phys. Rev. **D43**, 1763 (1991).
- [86] M. Gockeler, R. Horsley, P. E. Rakow, G. Schierholz, and H. Stuben, Nucl. Phys. Proc. Suppl. **34**, 527 (1994).
- [87] M. Gockeler, R. Horsley, P. E. Rakow, and G. Schierholz, Nucl. Phys. Proc. Suppl. **34**, 531 (1994).
- [88] M. Gockeler, R. Horsley, V. Linke, P. E. Rakow, G. Schierholz, *et al.*, Phys. Rev. Lett. **80**, 4119 (1998).
- [89] M. Gockeler, R. Horsley, E. Laermann, U. Wiese, P. E. Rakow, *et al.*, Phys. Lett. **B251**, 567 (1990).
- [90] M. Gockeler, R. Horsley, E. Laermann, P. E. Rakow, G. Schierholz, *et al.*, Nucl. Phys. **B334**, 527 (1990).
- [91] J. Kogut, E. Dagotto, and A. Kocic, Phys. Rev. Lett. **60**, 772 (1988).
- [92] P. E. Rakow, Nucl. Phys. **B356**, 27 (1991).
- [93] K.-I. Kondo, T. Iizuka, E. Tanaka, and T. Ebihara, Phys. Lett. **B325**, 423 (1994).
- [94] F. T. Hawes, T. Sizer, and A. G. Williams, Phys. Rev. **D55**, 3866 (1997).
- [95] F. T. Hawes, T. Sizer, and A. G. Williams, (1996).